Shape transformations of the aggregates in dilute surfactant solutions : a small-angle neutron scattering study

G. Porte, J. Marignan, P. Bassereau, R. May

Classification
Physics Abstracts
82.70 — 61.10D — 61.30E

Shape transformations of the aggregates in dilute surfactant solutions : a small-angle neutron scattering study

G. Porte, J. Marignan, P. Bassereau and R. May (*)

Groupe de Dynamique des Phases Condensées and GRECO Microemulsion, U.S.T.L., place E. Bataillon, 34060 Montpellier Cedex, France
(*) Institut Max von Laue-Paul Langevin, BP 156X, 38042 Grenoble Cedex, France

(*Reçu le 28 juillet 1987, révisé le 10 novembre 1987, accepté le 13 novembre 1987*)

Résumé. — Le coin riche en eau des diagrammes de phases des systèmes quasi ternaires tensioactif/alcool/eau salée fait apparaître les zones de stabilité de trois phases distinctes : la phase micellaire classique L_1, la phase lamellaire gonflée L_α, et une phase isotrope aux propriétés physiques assez particulières notée ici L_2^*. Les transformations de phase successives sont contrôlées par la valeur du rapport alcool/tensioactif. On rapporte ici une étude détaillée en diffusion des neutrons aux petits angles des transformations de forme des agrégats qui accompagnent les changements de phases. La séquence de formes suivante a été mise en évidence sans ambiguïté : globules, cylindres allongés, et finalement bicouches larges. Les structures primaires ont la même morphologie (larges bicouches) à l'échelle locale dans les deux phases L_α et L_2^*. Seul l'arrangement à grande échelle change de L_α à L_2^*. Les profils de diffusion à très petits q de L_2^* suggèrent que cette phase a une structure de topologie bicontinue ou une bicouche infinie sépare deux milieux eau salée identiques imbriqués l'un dans l'autre.

Abstract. — The brine rich corner of the phase diagrams of quasiternary (surfactant/alcohol/brine) systems shows the domains of stability of three different phases : the classical micellar phase L_1, the highly swollen lamellar phase L_α and an isotropic phase with quite special physical properties herein denoted L_2^*. The successive phase transformations are triggered by increasing values of the alcohol/surfactant ratio. We here report an extensive small angle neutron scattering investigation of the morphological transformations of the aggregates all along the phase sequence. The following shape sequence is unambiguously evidenced : globules, rods and finally wide bilayers. The primary structures have the same morphology at a local scale (bilayers) in both the L_α and L_2^* phases. Only the large scale arrangement of this elementary object changes from L_α to L_2^*. The very low q scattering patterns of L_2^* suggest that the structure of this phase has a bicontinuous topology where the infinite bilayer separates two infinite interwoven equivalent self-connected brine domains.

1. Introduction.

The polymorphism of the primary surfactant structures in binary (surfactant/water) or ternary (surfactant/alcohol/water) systems is well admitted : it is clearly indicated by the wide variety of ordered phases (lamellar, hexagonal, rectangular, nematic, cubic...) which usually appear in concentrated mixtures of such systems [1, 2]. In these well ordered concentrated phases, the long range orientational and positional orders can be characterized by X-ray scattering experiments. Then it is usually possible to derive the main features of the shape of the primary objects that are compatible with the measured positional periodicities.

The situation is not so clear in the dilute range. One still expects that morphological transformations also occur under these conditions but unambiguous evidences of these are far more difficult to obtain. In dilute mixtures, the aggregates are loosely packed and the intermicellar interactions are usually not strong enough to induce long-range positional order. But still, they are not weak enough to be neglected in the analysis of the scattering pattern of the studied mixture. To derive the micellar size and shape one has to treat both the form factor and the interference

function in a self-consistent procedure (such as in the Hayter-Penfold data treatment [3]). This is a very tough problem which has been solved only in the case of an interaction potential with spherical symmetry. The approach is useless in the case of a wide micellar polymorphism. The other way to reach the micellar morphology is to extrapolate the scattering data down to zero concentration. The problem is then that often the micellar shape changes with the dilution and sometimes turns back to the minimum globular shape at very high dilution.

One meets a much more favorable situation with common ternary ionic surfactant-alcohol aqueous mixtures when brine rather than pure water is used as the aqueous solvent. The most striking property of the obtained systems is that, even at very large dilutions, three different phases are successively stable for increasing relative alcohol contents [4]. Quite generally the phase sequence (Figs. 1 and 2) is the following. The isotropic micellar phase L_1 takes place at lower alcohol to surfactant ratio (ϕ_A/ϕ_S). At higher ϕ_A/ϕ_S, one meets the domain of stability of the swollen L_α lamellar phase. Very close to the domain of L_α, one finds along the alcohol rich side a very thin region of existence for an isotropic phase which is here denoted L_2^* like in [5].

Such phase transformations at a macroscopic scale most probably correspond to strong morphological transformations for the surfactant aggregates. We therefore expect for these systems a wide micellar polymorphism even at high dilution where intermicellar interactions are presumed to be very weak. Moreover, the radial geometry of the brine rich corner of the diagrams (Figs. 1, 2) indicates that the phase transformations occur for given values of ϕ_A/ϕ_S (where ϕ_A and ϕ_S are the respective volume fractions of the alcohol and of the surfactant) which do not depend on the dilution ϕ_w (where ϕ_w is the volume fraction of the brine). One therefore expects that the shape transformations of the primary structures are also mainly determined by ϕ_A/ϕ_S and

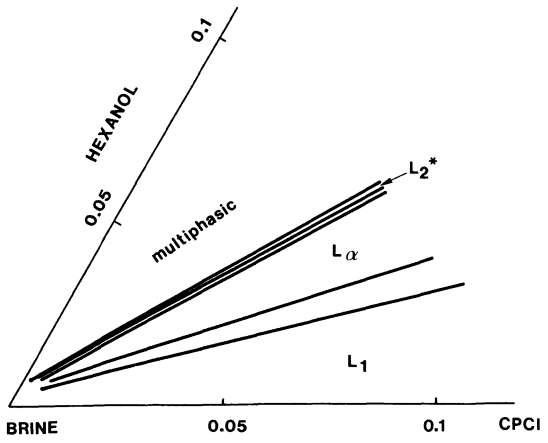

Fig. 1. — Brine rich corner of the phase diagram of the system CPCl/hexanol/brine.

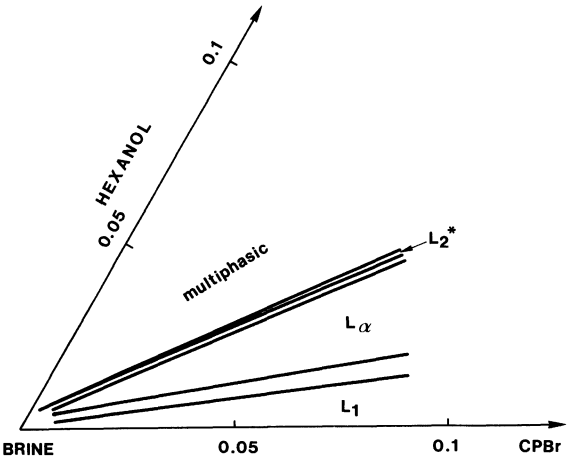

Fig. 2. — Brine rich corner of the phase diagram of the system CPBr/hexanol/brine.

almost insensitive to the dilution ϕ_w. Under these conditions structural information obtained at any given dilution in the dilute range should remain valid on a wide range of ϕ_w ($0.8 < \phi_w < 0.99$).

Here we take advantage of these opportunities to investigate the shape transformations of the aggregates in brine-rich mixture of quasi-ternary systems alcohol/surfactant/brine (we here consider the brine as a single component). Two similar systems are studied, namely cetylpyridinium chloride (CPCl)/*n*-hexanol/brine (0.2 M NaCl) and cetylpyridinium bromide (CPBr)/*n*-hexanol/brine (0.2 M NaBr). Since we deal with structural information, small-angle neutron and X-ray scattering are the main techniques of investigation. But also some viscosity and conductivity data are presented when they help to discriminate between alternative plausible models.

2. Experimental procedures.

The used chemical species (surfactant, hexanol, salts) are the same as in [5]. The brines are obtained by dissolution of the adequate amount of the salts in D_2O (99.8 % deuterium).

The phase behaviours (Figs. 1, 2) for the two systems are determined at 30 °C with the same observation methods as in [5]. The phase boundaries are found exactly identical when going from protonated brine [5] to deuterated brine once the compositions are expressed in mole fractions. So there is no noticeable isotopic effect at this level. A similar phase sequence is indeed found for the two systems, the only difference being that the phase transformations are triggered at lower ϕ_A/ϕ_S for the CPBr system than for the CPCl system. This special counterion effect is discussed in [6].

The structures of the L_1 and L_2^* isotropic phases were investigated using neutron scattering. The experiments were performed at the camera D11 of

the Institut Laue Langevin in Grenoble. Most scattering patterns were collected for dilute samples ($\phi_w > 0.96$) in the medium q-range which is adequate to investigate typical micellar dimensions.

The quartz sample cells (Hellma) had a pathway of 2 mm. An area of 1 cm^2 was illuminated by the neutron beam. The measured intensities were obtained on an absolute scale by adequate subtraction of the solvent and empty cell contributions, and by direct comparison with the intensity scattered incoherently under the same conditions by a 1 mm thick cell filled with H_2O [7]. Within the investigated q range ($q < 1.5 \times 10^{-1}$ Å^{-1}) the maximum relevant spatial resolution is about 10 Å and it is not necessary to specify the scattering length density distribution in the object at the finer scale. The data treatment is then based on only one contrast factor between the active matter and the deuterated brine solvent. In order to estimate the contrast factor consistently, the densities of the surfactant and of the hexanol are needed. The density of the hexanol in the micelles is assumed to be the same as in the pure liquid phase (= 82) and the density of the micellized surfactant is derived from the evolution of the density of the binary surfactant brine mixture as a function of ϕ_w (linear dependence). It is assumed to be independent of the effective alcohol to surfactant ratio in the micelles. Lastly, the fast exchange between the initial protonated OH groups of the hexanol and the deuteriums of the heavy brine solvent is taken into account (this effect is certainly not negligible in the estimation of the mass of the micellar object).

In order to get some insight into the L_2^* large scale arrangement some scattering patterns were collected for more concentrated samples ($0.8 < \phi_w < 0.98$) on a much wider q range (3×10^{-3} Å$^{-1} < q < 1 \times 10^{-1}$ Å^{-1}). These data were obtained on the same instrument using successively various sample-to-detector distances : 2.5 m, 5.5 m and 10.5 m.

The more concentrated L_α mixtures (with average periodicities d in the range 50 Å $< d <$ 200 Å) were studied using the standard X-ray scattering set up of our laboratory. The sample consists of a cylindrical Lindemann capillary tube (diameter 1 mm) filled with the investigated mixture. The capillary walls are treated in sulfochromic acid in order to obtain the cylindrically symmetrical alignment of the bilayers [8]. The scattering set up here works in point collimation. Complementary data (photographs) were obtained on line D16 at the synchrotron light source in LURE. The more diluted L_α samples (with average periodicities in the range 200 Å $\leqslant d \leqslant$ 1 100 Å) are studied on D11 at the ILL. Here the requirement is to reach the scattering profile at very low q (large d) 10^{-3} Å$^{-1} < q < 5 \times 10^{-2}$ Å^{-1}, and sample-to-detector distances of 5.5 m, 10.5 m and 20.5 m are used depending on the dilution ϕ_w ($0.8 < \phi_w < 0.97$). In order to achieve a good cylindrically symmetrical alignment of the lamellar stacking, a parallel bundle of quartz cylindrical tubes (about 10 tubes-1 mm diameter) are introduced into the cell and imbedded into the L_α mixture.

3. Globules to rods transformation in the L_1 phase.

The physical property of the L_1 phase which varies most sensitively with the alcohol-to-surfactant ratio ϕ_A/ϕ_S is the viscosity of the mixture. The points denoted by full circles in figure 3 represent the relative viscosities of binary CPCl/brine mixtures at different concentrations. The points align nicely along a straight line with a moderate slope ($\Delta\eta_r/\Delta\phi_S \cong 3$) which is consistent with a nearly spherical shape for globular micelles.

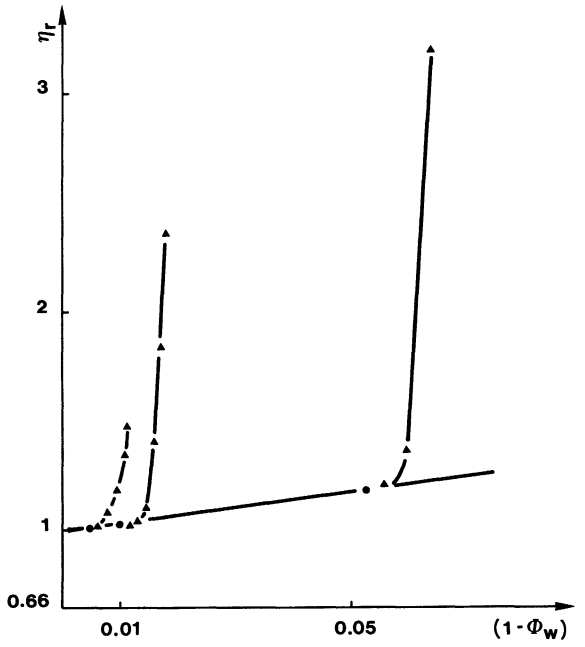

Fig. 3. — Relative viscosity η_r of the L_1 phase of the CPCl system *versus* $(1 - \phi_w)$. Full circles : binary mixtures (CPCl/brine). Full triangles : progressive addition of hexanol.

The Guinier ($\ln I(q)$ *vs.* q^2) plot of the scattering profile of a 0.01 g/cm^3 CPCl brine mixture is used to check this structural model (Fig. 4). For a random

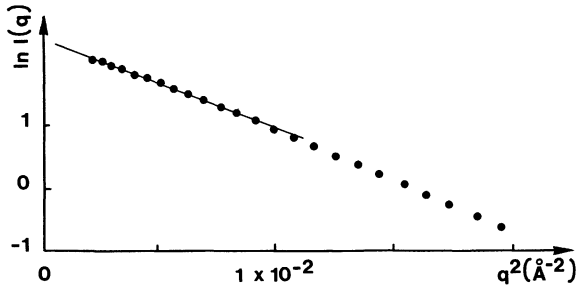

Fig. 4. — Guinier plot of $I(q)$ (neutrons) for globular CPCl micelles (sample composition : $c_w = 0.99$, $\phi_A/\phi_S = 0$, where c_w is the mass fraction of the brine).

distribution of globular objects one expects the scattered intensity to scale as [9] :

$$I(q) = cM(b_m - V_m \rho_0)^2 \exp(-R_G^2 q^2/3) \quad (1)$$

at small $q(qR_G \leqslant 1)$ where R_G is the radius of gyration of the particle, c is the concentration of the sample (g/cm^3), M is the mass of the particle (g) and $(b_m - V_m \rho_0)$ is the contrast difference between the particle and the solvent (cm/g). Neglecting intermicellar interactions (diluted sample, high salt brine) we treat the data of figure 4 according to (1). Doing so we obtain : $R_G = 19.6 \pm 1$ Å and $M = 6.6 \pm 0.5 \times 10^{-20}$ g. Assuming that the micelles are perfect homogeneous spheres, we can deduce from the R_G and M values two different estimate r_{0g} and r_{0m} of the radius of the equivalent sphere. We obtain $r_{0g} = 26 \pm 1$ Å and $r_{0m} = 25.5 \pm 1$ Å. These two very similar values should be compared to the average hydrodynamic radius R_H of CPCl micelles as measured under similar conditions by quasi elastic light scattering : $R_H \cong 29$ Å ± 1 Å. The difference is small (about 3 Å) and is most probably related to the fact that R_H is a measure of the radius of the hydrated micelle while r_{0g} and r_{0m} are the radius of the dry equavalent sphere (the bound D_2O molecules have no contrast with the free solvent and do not contribute to the scattering pattern).

As shown in figure 3 (full triangles) addition of hexanol induces at all concentrations a very steep increase of the relative viscosity of the mixture which is not consistent with the globular description. The viscosities of CPBr/brine binary mixtures are also much too large to be consistent with a globular shape for the micelles even when no alcohol is added. In all these cases, the Guinier plot used above fails to exhibit the straight decay expected for globules. On the other hand, the plot of ln $(q \,.\, I(q))$ *versus* q^2 does exhibit a linear decay over a large q range (Fig. 5). Such q^{-1} dependence for $I(q)$ is characteristic of rod-like objects [10]. More precisely, for a random distribution of rod-like particles one expects $I(q)$ to vary as :

$$q \,.\, I(q) = \pi C M_L (b_m - \rho_0 V_m)^2 \times \times \exp(-R_c^2 q^2/2) \quad (2)$$

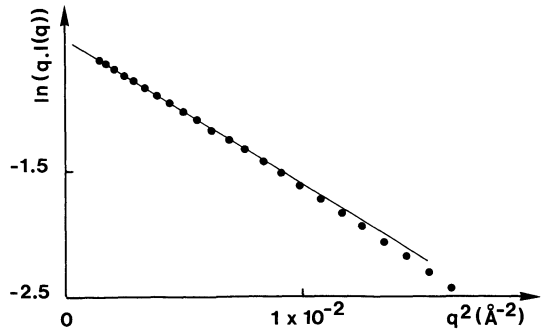

Fig. 5. — ln $[ql(q)]$ *versus* q^2 for CPBr cylindrical micelles (sample composition $c_w = 0.99$, $\phi_A/\phi_S = 0$).

in the range $qR_c < 1$ and $q\langle l \rangle \geqslant 1$ where R_c is the radius of gyration of the normal section of the rod and $\langle l \rangle$ is the persistence length i.e. the average length below which the linear object can be considered as straight and rigid. In [2] M_L is the mass per unit length of the object. From the $I(q)$ dependence in the range 3×10^{-2} Å$^{-1} < q < 1.5 \times 10^{-1}$ Å^{-1} we deduce R_c and M_L for different high viscosity L_1 samples of both CPBr and CPCl systems (Tab. I). From R_c and M_L we derive two separate estimates of the radius of the equivalent circular cylinder r_{0g} and r_{0m}. We obtain $r_{0g} \cong r_{0m} \cong 20$ Å for the CPCl samples and $r_{0g} \cong r_{0m} \cong 22$ Å for the CPBr samples.

Table I. — *Characteristic sizes of the cylinder normal section of the elongated* CPBr *and* CPCl *micelles. For the* CPBr $\phi_w = 0.99$ *sample a failure of the preset counter occurred and the absolute scale data treatment could not be achieved.*

Sample			Characteristic size		
	c_w	c_A/c_S	$r_{0,g}$ (Å)	M_L (g/cm)	$r_{0,m}$ (Å)
CPCl	0.985	0.55	19.6	1.12×10^{-13}	19.7
CPCl	0.935	0.3	19.5	1.21×10^{-13}	20.4
CPBr	0.99	0	22.2	?	?
CPBr	0.988	0.17	22.3	1.56×10^{-13}	21.7

In order to make significative comparisons, we have also measured by X-ray scattering the average periodicities in the hexagonal phases which appear in much more concentrated regions of the phase diagrams of the two systems (Tab. II). From these data we derive $r_{0,hex}$ the dry radius of the cross-

Table II. — *Periodicities d and cylinder normal section* $r_{0,hex}$ *in the hexagonal phase of the* CPCl *and* CPBr *systems at high concentration.*

Sample			Characteristic size	
	c_w	c_A/c_S	$\bar{d}$ (Å)	$r_{0,hex}$ (Å)
CPBr	0.70	0	67.5	22.2
CPCl	0.58	0.14	55.2	21.6
CPCl	0.57	0.17	54.5	21.7
CPCl	0.56	0.20	54.6	21.9

section of the equivalent circular cylinders in these concentrated phases. Significantly, for all samples the value of $r_{0,\,hex}$ (≈ 22 Å ; Tab. II) is similar to $r_{0,\,g}$ and $r_{0,\,m}$ indicating that the long micelles in the diluted L_1 phase and in the concentrated hexagonal phase have the same local structure.

The occurrence of cylindrical micelles rather than lamellar micelles (disks) while approaching a « compact » lamellar phase (see next section) is quite surprising and deserves further examination. Data at much lower q (5×10^{-3} Å$^{-1} < q < 5 \times 10^{-2}$ Å^{-1}) have been collected. At very low q the effect of the finite radius of the cylinders or the finite thickness of the eventual lamellae on the $I(q)$ profile is negligible and one expects simply $I(q) \sim q^{-1}$ for rods and $I(q) \sim q^{-2}$ for disks. We obtained an exact q^{-1} dependence down to $q \sim 1.5 \times 10^{-2}$ Å^{-1} with a slight upward deviation at lower q (5×10^{-3} Å$^{-1} < q < 1.5 \times 10^{-2}$ Å^{-1}). The deviation is classically interpreted in polymer science [9] as related to the finite rigidity of the rods. So finally, the *rod model with some flexibility* [11] *fits the data in absolute units* in the entire 5×10^{-3} Å$^{-1} < q < 1.5 \times 10^{-1}$ Å^{-1} range and we verify easily that the disk model is totally inapropriate.

4. Compact bilayers in the L_α phase.

The most enigmatic property of the L_α phase of both systems is certainly the exceptional stability of its long range order at high dilution. It remains definitely birefringent up to $\phi_w \cong 0.995$ (orientational order) and exhibits focal conics textures up to at least $\phi_w \cong 0.96$. We do not discuss here this point which is now the field of intense theoretical and experimental investigations [8, 12-15]. We rather use the regularity of the lamellar stacking in order to derive the essential features of the morphology of the individual bilayers.

Figure 6 represents the 2D-photographic recording of the scattering pattern of a moderately swollen CPCl L_α sample ($d = 98$ Å). It essentially consists of two symmetrical well defined spots corresponding to the first Bragg singularity associated with the regularity of the stacking. The important point to note is the fact that these Bragg patches have a very small extention in the direction q normal to the director of the phase. This pattern is the direct indication [16] that the individual lamellae are homogeneous, compact and do not present a noticeable density of structural defects such as pores or fractures. More precisely, the average in plane distance between possible structural defects or heterogeneities is certainly larger than several 10^3 Å. This homogeneous and regular structure of the individual bilayers has been further confirmed for the CPCl L_α phase using ESR technique on well oriented homeotropic samples [17].

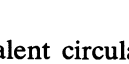

Fig. 6. — 2D photographic recording of the scattering pattern of a CPCl L_α mixture with $c_w = 0.75$.

We derive the average thickness d_0 of the bilayers from the evolution of the Bragg peak position q_B as a function of ϕ_w. For constant d_0 we expect the linear relation :

$$q_B = 2\,\pi / d_0 (1 - \phi_w) \,. \qquad (3)$$

Figure 7 shows the scattering patterns of CPCl L_α sample at various dilutions. Even for very large interlamellar distances d (Fig. 7b ; $d \approx 970$ Å) the Bragg maximum remains well defined. The expected linear dependence (3) is very well confirmed on an

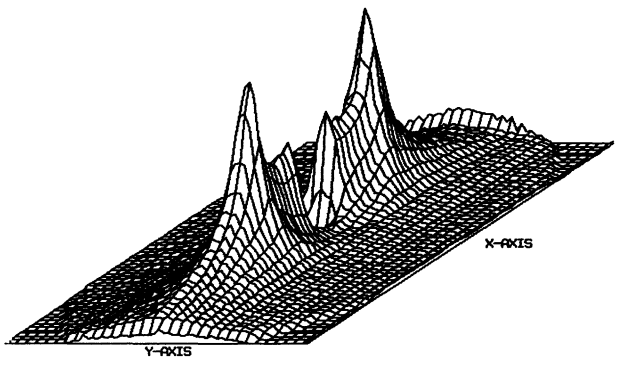

a)

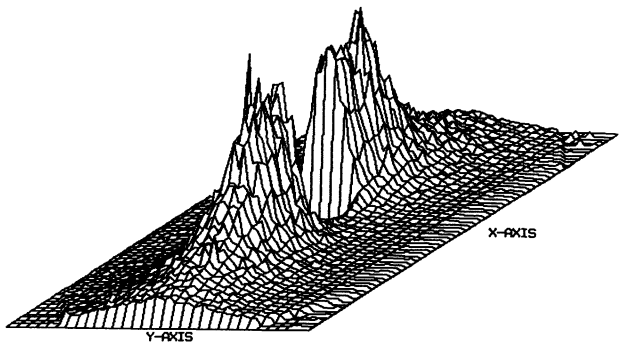

b)

Fig. 7. — a) 2D scattering pattern of a CPCl L_α mixture with d : 200 Å (neutrons) sample to detector distance : 2.5 m. b) 2D scattering pattern of a CPCl L_α mixture with d : 970 Å (neutrons) ; sample to detector distance : 10.5 m.

exceptionally large range of dilution (Fig. 8) and d_0 of CPCl L_α bilayers :

$$d_{0\,\mathrm{CPCl}} = 26.5 \pm 1 \text{ Å}$$

is found.

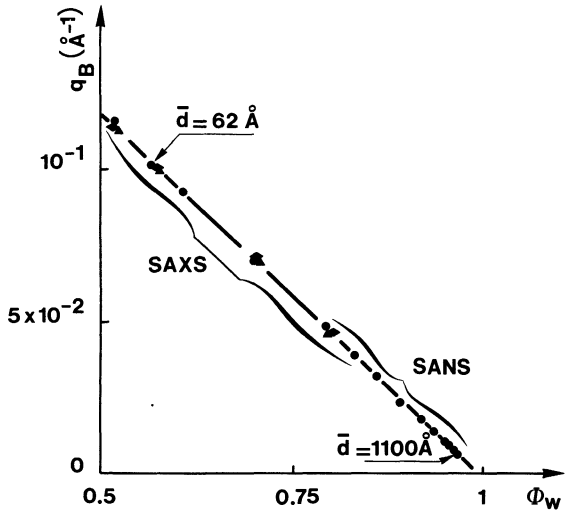

Fig. 8. — Bragg peak position q_B *versus* ϕ_w for the L_α phase.

The same treatment of a smaller set of data on the CPBr system (50 Å $\leq d \leq$ 200 Å) gives a quite similar value [6] :

$$d_{0\,\mathrm{CPBr}} = 27.5 \pm 1 \text{ Å} .$$

5. L_2^* : large bilayers with no long range order.

L_2^* is an isotropic phase with quite special physical properties. In particular it shows a very noticeable transient optical birefringence upon gentle stirring [4]. This property is not so unique in itself [18], but very surprising is the fact that it becomes stronger and stronger when the dilution ϕ_w increases. In the same manner, the intensity of the light scattered by the phase increases with ϕ_w and diverges at $\phi_w \to 1$. (Quantitative data on these two properties will be reported in a forthcoming paper.)

Figure 9 shows the variations of the conductivity σ of L_2^* with ϕ_w. Very remarkably, the extrapolation of σ to zero concentration in active matter is significantly different from σ_0, the conductivity of the pure brine solvent. We have approximately :

$$\lim \sigma \approx 2/3\ \sigma_0 \qquad (4)$$

which means that the L_2^* surfactant structure opposes a constant *finite* obstruction to the mobility of the free ions at high dilution.

We investigate the structure on dilute samples ($\phi_w \cong 0.96$ and $\phi_w \cong 0.98$) using again neutron scattering in the medium q range. As a matter of

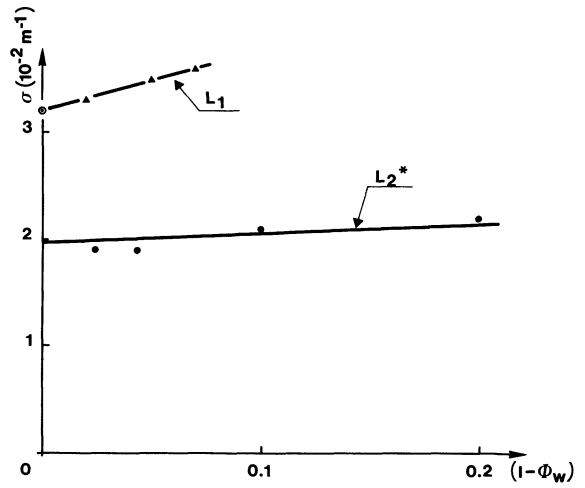

Fig. 9. — The conductivity σ as function of $(1 - \phi_w)$, full triangles : L_1 phase, full circles : L_2^* phase.

fact, the Guinier plots, which were found efficient in the different specific situations in L_1 (globules, rods), here both fail to exhibit a straight decay within this q-range. On the other hand the plot $\ln (q^2 I(q))$ *versus* q^2 (Fig. 10) shows a nicely linear

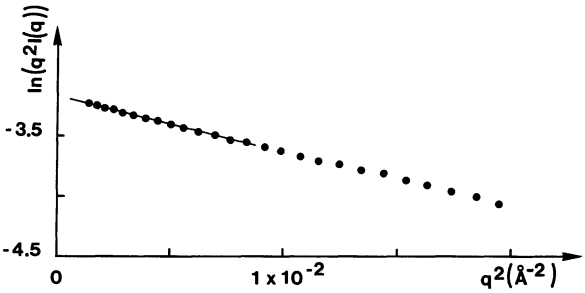

Fig. 10. — $\ln (q^2 I(q))$ *versus* q^2 for the L_2^* CPCl mixture with the composition $c_w = 0.977$; $c_A/c_S = 1.25$ (c_A and c_S are the mass fractions of the alcohol and of the surfactant).

decay. The situation is nevertheless not as clear as in L_1 since the q^{-2} dependence of $I(q)$ is not specific of one only local structure [10]. In the present case, it could correspond to any of the three following different structural models : i) Gaussian coils built up with elementary units of about 20 Å size ; ii) critical fluctuations in a dispersion of micelles of about 16 Å radius and iii) large flat bilayers of about 25 Å thickness randomly oriented within the sample. The situation is specially confusing since all three possibilities involve sizes equally plausible for the self-aggregation of surfactant molecules. The particular behaviour of the conductivity helps to discriminate between them. For Gaussian coils or critical dispersion of micelles we indeed expect σ to reach σ_0 asymptotically at high dilution. On the other

hand Jonsson *et al.* have explicitly computed the obstruction factor for randomly oriented infinite flat aggregates [19] and they found that it is precisely equal to 2/3. And the variation of σ with ϕ_w is a strong indication for the third structural description.

To check this local structure further, we have treated the neutron data in *absolute units*. For a random dispersion of large flat platelets one expects $I(q)$ in the medium q-range to vary according to [9] :

$$q^2 I(q) = 2\pi^2 c M_A \cdot (b_m - \rho_0 V_m)^2 \times \times \exp(-q^2 d_{0g}^{*2}/12) \quad (5)$$

where M_A is the mass per unit area of the bilayer and d_{0g}^* is its apparent dry thickness (as derived from the one-dimensional radius of gyration of the scattering length density along the normal to the layer [9]). This expression in principle allows for two seperate determinations of d_0^* : namely d_{0g}^* from the slope of the log plot in figure 10 and d_{0m}^* from the value of M_A which is obtained by extrapolation of $q^2 I(q)$ to zero-q. The obtained values (d_{0g}^*, M_A and d_{0m}^*) for different samples are given in table III. For each sample, d_{0g}^* and d_{0m}^* are similar within an accuracy better than 10 %.

Table III. — *Characteristic sizes of the thickness of the bilayers in the L_2^* phase. A phase separation occurred in the* CPBr *sample (L_2^*/L_1) during the experiment which made impossible the absolute scale data treatment.*

Sample			Characteristic size		
	c_w	c_A/c_S	$d_{0,g}^*$ (Å)	M_A (g/cm^2)	$d_{0,m}^*$ (Å)
CPCl	0.977	1.25	24.2	2.1×10^{-7}	23.1
CPCl	0.962	1.12	22.1	2.09×10^{-7}	23.5
CPBr	0.982	0.8	25.1	?	?

Here we have not investigated in detail the effect of the concentration on the effective values of d_{0g}^*. However, clearly for the CPCl system, d_{0g}^* is smaller for the $\phi_w \cong 0.96$ sample than for the $\phi_w \cong 0.98$ sample. The positional correlations between the primary flat structures are thus not completely negligible even at this rather high dilution. A straight forward extrapolation of these two values down to zero concentration in active matter indicates an actual value for the thickness of the layer in this system between 25 and 26 Å. So d_0^* in the L_2^* phase is comparable to d_0 in the L_α phase suggesting that, at a local scale, the bilayer has the same structure in both phases.

6. Discussion.

Here we present a clear experimental evidence that the aggregates in dilute solutions transform from globules into long cylinders and finally into large bilayers upon progressive addition of alcohol. Interestingly this shape sequence corresponds to a smaller and smaller total curvature for the surfactant alcohol film and agrees with the now well admitted empirical principle stating that addition of alcohol decreases the spontaneous curvature of the surfactant alcohol film [20].

But although unambiguous, the obtained shape descriptions remain quite coarse. They are derived from low q scattering data ($q < 1.5 \times 10^{-2}$ Å^{-1}) and details of the structure involving lengths smaller than a few nm will be smeared out by the low spatial resolution of the data. At the present time we cannot state anything about the eventual anisometry and the polydispersity of the globules or the eventual ellipticity of the orthogonal section of the cylinders for instance.

An important result of our study is to show that, at a *local scale,* the surfactant aggregates have a similar morphology in L_α and in L_2^*. So between these two phases only the large scale arrangement of a common local scale structure changes. There are at least four different large scale arrangements for bilayers that could correspond to the L_2^* isotropic phase. What differs from one to the other is mainly the topology of the structure. The first one is derived from L_α assuming that addition of hexanol results in disrupting the infinite layers into finite-size, disk-shape micelles. The corresponding topology is that of a direct micellar phase. The second model is based on the idea that bilayers connect to each other along junction lines generating a « foam like arrangement ». The corresponding topology is that of the inverse micellar phase : the brine microdomains are entrapped within the « bubbles » of the « foam » while the walls consist of the surfactant bilayer which is self connected throughout the sample [5]. The third model has the same topology as the L_α lamellar phase. It is derived from the L_α structure assuming that addition of hexanol results in the spontaneous formation of a large density of defects such as dislocations and disclinations. The long-range orientational and positional orders could then collapse into short-range orders with finite correlation lengths as proposed by Parodi in [21]. We refer to this model as to the « locally lamellar » model. The last topology is suggested by the extensive literature on bicontinuous microemulsions. In these mixtures the water and the oil media are assumed to be self-connected throughout the sample and separated by the surfactant film [22, 23]. By analogy, we assume in this model that the bilayer in L_2^* has the same topology as the surfactant film in bicontinuous

microemulsions : it separates two identical — self connected and mutually disconnected — brine medias. We refer to this model as to the « bicontinuous model ».

Neutron scattering data have been collected for four L_2^* samples with the dilutions : $c_w = 0.80$, 0.86, 0.91 and 0.96 (where c_w is the mass fraction of the brine) in the q-range 3×10^{-3} Å$^{-1} < q < 1.5 \times 10^{-1}$ Å^{-1}. For all samples, the scattering profiles show (Fig. 11) an abrupt slope variation at a certain value q_c of q (Tab. IV). For the two most concentrated samples a maximum of $I(q)$ is observed

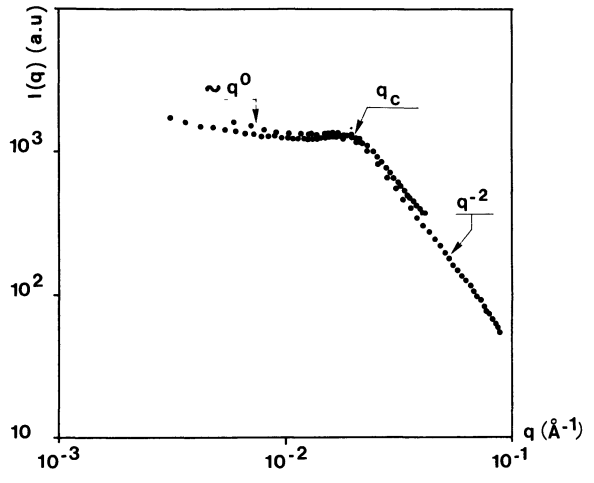

Fig. 11. — ln $I(q)$ *versus* ln q in the range 3×10^{-3} Å$^{-1} < q < 1 \times 10^{-1}$ Å^{-1} for the L_2^* CPCl sample with $c_w = 0.91$ and $c_A/c_S = 1.05$.

Table IV. — *Variation of the position q_c of the maximum of $I(q)$ in L_2^* as function of $(1 - \phi_w)$ and corresponding values of d^*.*

$1 - \phi_w$	q_c (Å^{-1})	d^* (Å)
0.044	7.4×10^{-3}	850
0.108	1.8×10^{-2}	340
0.162	3.0×10^{-2}	210
0.223	4.2×10^{-2}	150

(Fig. 12) at q_c. Comparing q_c in L_2^* with the Bragg wave vector q_B in the L_α phase at the same dilution shows that they are of the same order at all dilutions. It is then reasonable to interpret q_c as the signature of the average distance d^* between bilayers in the L_2^* structure and to assume that $q_c = 2\pi/d^*$.

Plotting q_c as a function of ϕ_w we obtain a straight line. With $d_0^* \approx 25$ Å as measured in a preceding section the corresponding relation between d^* and ϕ_w can be written :

$$d^* = \alpha \cdot d_0^* (1 - \phi_w)^{-1} \qquad (6)$$

with $\alpha \approx 1.4 \pm 0.1$.

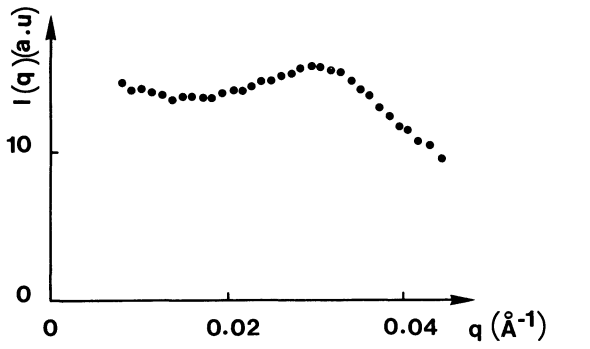

Fig. 12. — $I(q)$ for the ($c_w = 0.86$; $c_A/c_S = 1.03$) sample. A broad hump is easily observed.

For disk micelles, (6) would imply that the size of the disks increases with ϕ_w, an expectation which is unrealistic within the frame work of self-aggregation thermodynamics. And we discard firmly a direct topology for the L_2^* structure.

The other three topologies considered involve bilayers connected over very large distances. d^* is then expected to be proportional to $(1 - \phi_w)^{-1}$ in all three cases. But each topology corresponds to a typical value of the constant α in relation (6). In order to estimate the different α values we have found it convenient to use the following procedure. First we draw a simple cubic lattice with unit cell of size d^*. Then we force the bilayer to lie on the surface of the cubic cells [23]. Depending on the particular topology an average number N out of the six faces of each unit cubic cell will be covered by the bilayers. One easily verifies that α is then simply : $\alpha = N/2$. Apart from its convenience, this procedure enlightens the intimate relation between the value of α and the average degree of connection between adjacent small brine domains of size d^* in the structure.

For the foam-like structure each cell is totally disconnected from its neighbours. Then $N = 6$ and $\alpha = 3$. In the locally lamellar structure the bilayers are stacked parallel to each other at a distance d^*. This corresponds on the cubic lattice to $N = 2$ and indeed $\alpha = 1$ (as in relation (3)). To illustrate what could be expected in the case of a bicontinuous topology we have drawn on the cubic lattice the particular structure represented in figure 13. For this structure, one counts out $N = 3$; so $\alpha = 1.5$.

The experimentally determined value of α for L_2^* ($\alpha \approx 1.4$) is significantly different from the values expected for the foam ($\alpha = 3$) and for the locally lamellar structure ($\alpha = 1$). On the other hand the agreement with the value calculated for the bicontinuous model seems quite good. Indeed this does not mean that figure 13 actually represents the structure of L_2^*. But this means that the average degree of connection between brine cells of size d^* in L_2^* and in the bicontinuous model is about the

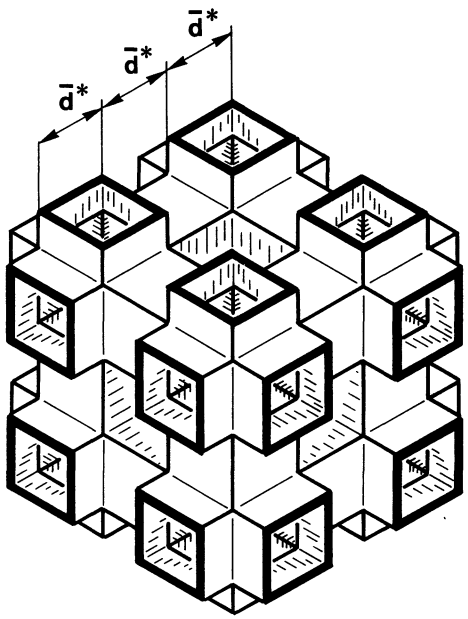

Fig. 13. — An example of bicontinuous structure drawn on the simple cubic lattice with unit cells of size d^*.

same, suggesting that both structures have the same topology. One also verifies easily that the conductivity at high dilution of the model is in between $0.5 \times \sigma_0$ and $0.75 \times \sigma_0$ in agreement with the measured value $0.6 \times \sigma_0$. Here again, we guess that any other structural model having the same topological properties should have a similar conductivity.

To sum up the discussion, we conclude that the direct topology (disk micelles), the inverse topology (foam) and the lamellar topology (locally lamellar structure) all seem to be improbable for the structure of the L_2^* phase. On the other hand, a bicontinuous topology where the bilayer separates two interwoven equivalent self-connected brine domains seems to be more plausible in view of our present results.

Acknowledgments.

We thank J. Charvolin and D. Roux for illuminating discussions on bicontinuous structures. This research has received partial financial support from a PIRSEM (CNRS) grant n° AIP 2004.

References

[1] EKWALL, P., *Advances in Liquid Crystals,* Ed. G. M. Brown (Academic, New York) 1975.

[2] SKOULIOS, A., *Ann. Phys.* **3** (1978) 421.

[3] HAYTER, J. B., PENFOLD, J., *Mol. Phys.* **42** (1981) 109.

[4] BENTON, W. J., MILLER, C. A., *J. Phys. Chem.* **87** (1983) 4981.

[5] PORTE, G., GOMATI, R., EL HAITAMI, O., APPELL, J., MARIGNAN, J., *J. Phys. Chem.* **90** (1986) 5746.

[6] GOMATI, R., APPELL, J., BASSEREAU, P., MARIGNAN, J., PORTE, G., to appear in *J. Phys. Chem.*

[7] JACROT, B., ZACCAI, G., *Biopolymers* **20** (1981) 2413.

[8] BASSEREAU, P., MARIGNAN, J., PORTE, G., *J. Phys. France* **48** (1987) 673.

[9] GLATTER, O., KRATKY, O., *Small Angle X-rays Scattering* (Academic Press, New York) 1982.

[10] CABANE, B., « Small Angle Scattering Methods » in *Surfactant Solutions : new methods of investigation,* Surfactant science series Vol. **22,** Ed. R. Zana (Marcel Dekker) 1986.

[11] PORTE, G., APPELL, POGGI, Y., *J. Phys. Chem.* **84** (1980) 3105.
APPELL, J., PORTE, G., POGGY, Y., *J. Colloid Interface Sci.* **87** (1982) 492.

[12] HELFRICH, W., *Z. Naturforsch* **33a** (1978) 305.

[13] SAFINYA, C. R., ROUX, D., SMITH, G. S., SINHA, S. K., DIMON, P., CLARK, N. A., BELOCQ, A. M., *Phys. Rev. Lett.* **57** (1986) 2518.

[14] LARCHE, F. C., APPELL, J., PORTE, G., BASSEREAU, P., MARIGNAU, J., *Phys. Rev. Lett.* **56** (1986) 1700.

[15] LIPOWSKI, R., LEIBLER, S., *Phys. Rev. Lett.* **56** (1986) 2541.

[16] HOLMES, M. C., CHARVOLIN, J., *J. Phys. Chem.* **88** (1984) 810.

[17] DI MEGLIO, J. M., BASSEREAU, P., unpublished results.

[18] See for instance, ULMIUS, J., WENNERSTROM, H., JOHANSSON, L. B., LINDBLOM, G., GRAVSHOLT, S., *J. Phys. Chem.* **83** (1979) 2232.

[19] JONSSON, B., WENNERSTROM, H., NILSSON, P. G., LINSE, P., *Colloid Polymer Sci.* **264** (1986) 77.

[20] HENDRICKX, Y., CHARVOLIN, J., RAVISO, M., *J. Colloid Interface Sci.* **100** (1984) 597.
ALPERINE, S., HENDRIKX, Y., CHARVOLIN, J., *J. Phys. Lett. France* **46** (1985) L27.
MATHER, D. E., *J. Colloid Interface Sci.* **57** (1976) 240.

[21] PARODI, O., *Colloides et Interfaces,* Ed. A. M. Cazabat et M. Veyssie (Les Editions de Physique) 1984.

[22] TALMON, Y., PRAGER, S., *J. Chem. Phys.* **69** (1978) 2984 ;
SCRIVEM, L. E., *Nature* **263** (1976) 123.

[23] DE GENNES, P. G., TAUPIN, C., *J. Phys. Chem.* **86** (1982) 2294.
JOUFFROY, J., LEVINSON, P., DE GENNES, P. G., *J. Phys. France* **43** (1982) 1241.